

Article

## Switchable Chiral Selection of Aspartic Acids by Dynamic States of Brushite

Wenge Jiang, Haihua Pan, Zhisen Zhang, S. Roger Qiu, J. Dongun Kim, Xurong Xu, and Ruikang Tang

*J. Am. Chem. Soc.*, **Just Accepted Manuscript** • Publication Date (Web): 07 Jun 2017

Downloaded from <http://pubs.acs.org> on June 7, 2017

### Just Accepted

“Just Accepted” manuscripts have been peer-reviewed and accepted for publication. They are posted online prior to technical editing, formatting for publication and author proofing. The American Chemical Society provides “Just Accepted” as a free service to the research community to expedite the dissemination of scientific material as soon as possible after acceptance. “Just Accepted” manuscripts appear in full in PDF format accompanied by an HTML abstract. “Just Accepted” manuscripts have been fully peer reviewed, but should not be considered the official version of record. They are accessible to all readers and citable by the Digital Object Identifier (DOI®). “Just Accepted” is an optional service offered to authors. Therefore, the “Just Accepted” Web site may not include all articles that will be published in the journal. After a manuscript is technically edited and formatted, it will be removed from the “Just Accepted” Web site and published as an ASAP article. Note that technical editing may introduce minor changes to the manuscript text and/or graphics which could affect content, and all legal disclaimers and ethical guidelines that apply to the journal pertain. ACS cannot be held responsible for errors or consequences arising from the use of information contained in these “Just Accepted” manuscripts.

# Switchable Chiral Selection of Aspartic Acids by Dynamic States of Brushite

Wenge Jiang,<sup>†,‡</sup> Haihua Pan,<sup>‡,‡</sup> Zhisen Zhang,<sup>†</sup> S. Roger Qiu,<sup>§</sup> J. Dongun Kim,<sup>||</sup> Xurong Xu,<sup>‡</sup> and Ruikang Tang<sup>\*,†,‡</sup>

<sup>†</sup> Center for Biomaterials and Biopathways, Zhejiang University, Hangzhou, Zhejiang, 310027, China

<sup>‡</sup> Qiushi Academy for Advanced Studies, Zhejiang University, Hangzhou, Zhejiang, 310027, China

<sup>§</sup> Physical and Life Sciences Directorate, Lawrence Livermore National Laboratory, Livermore, CA 94551, USA

<sup>||</sup> Department of Chemistry and Chemical Biology and Institute of Marine and Coastal Sciences, Rutgers, the State University of New Jersey, New Brunswick, NJ 08854, USA

## Supporting Information

**ABSTRACT:** We herein show the chiral recognition and separation of aspartic acid (Asp) enantiomers by achiral brushite due to the asymmetries of their dynamical steps in its non-equilibrium states. Growing brushite has a higher adsorption affinity to D-Asp, while L-Asp is predominant on dissolving brushite surface. Micro structural characterization reveals that chiral selection is mainly attributed to brushite [101] steps, which exhibit two different configurations during crystal growth and dissolution, respectively, with each preferring a distinct enantiomer due to this asymmetry. Because these transition step configurations have different stabilities, they subsequently result in asymmetric adsorption. By varying free energy barriers through solution thermodynamic driving force (i.e., supersaturation), the dominant non-equilibrium intermediate states can be switched and chiral selection regulated. This finding highlights that the dynamic steps can be vital for chiral selection, which may provide a potential pathway for chirality generation through the dynamic nature.

## INTRODUCTION

A most intriguing but unanswered scientific question relates to the origin of biochemical homochirality, which holds that only L-amino acids construct natural proteins.<sup>1-5</sup> Many chemists and geologists suggest that minerals might play a vital role in the origin of homochirality of biomolecules in the ancient ocean. Among those minerals, surfaces of chiral rock-forming minerals, such as quartz (SiO<sub>2</sub>), alkali feldspar ((Na,K)AlSi<sub>3</sub>O<sub>8</sub>), clinopyroxene ((Ca,Mg,Fe)SiO<sub>3</sub>), gypsum (CaSO<sub>4</sub>·2H<sub>2</sub>O) and calcite (CaCO<sub>3</sub>), have been studied intensively and scientists suggest that the adsorption of chiral organic molecules onto the chiral surfaces of these minerals may have induced the prebiotic chiral selection from the initially racemic soup,<sup>6-10</sup> which may trigger the predominance of homochirality by chiral amplification reaction.<sup>11,12</sup> Although the inherently chiral surfaces within these crystals may provide possible locations for chiral separation of amino acid, it has been argued that chiral minerals were likely not responsible for a global periodic excess of L-amino acids because the proportions of left- and right-chiral mineral surfaces in nature are equal.<sup>6,7,13-15</sup>

It has long been understood that one chiral mineral face or chiral step specifically selects one enantiomer of amino acids. Here, we found that chiral selection of aspartic amino acid (Asp) enantiomers can also be switched by the non-equilibrium state (growing or dissolving) of brushite (CaHPO<sub>4</sub>·2H<sub>2</sub>O; monoclinic, *Ia*),<sup>16,17</sup> a rock-forming mineral on Earth. Brushite is an acidic mineral, which has been suggested to be the first precipitated solid phase in the acidic ancient ocean;<sup>18,19</sup> and Asp is considered to play a pivotal role in the origin of life.<sup>20,21</sup> In fact, Asp is among the most abundant amino acids formed in experiments simulating amino acid formation on the primitive earth<sup>4</sup> and on the Murchison meteorite.<sup>20</sup> Of particular interest, Asp acidic amino acid residues of protein have as a hallmark feature the regulation of mineral morphologies by interfacial interactions in biomineralization processes.<sup>22</sup> The present study shows that the amount of D- or L-Asp enantiomer adsorbed onto brushite is quite different between growing and dissolving crystals - growing brushite prefers D-Asp, while L-Asp predominates on dissolving brushite. More broadly, considering the environmental change of ancient ocean chemistry before the formation of life in changing from slightly acidic to

neutral and being a critical period for the formation of biomolecules – which drove equilibrium states for rock-forming minerals to a non-equilibrium state<sup>18,19</sup> – a continuous demineralization state might accumulate dominant L-amino acids on the mineral-dissolving surfaces to break an originally chiral balance between enantiomers in the racemic system. The asymmetric interaction between dynamic brushite and D- or L-enantiomers may offer general insights into the important pathway for the selection of homochirality during the dynamic change of the chemical environment of the Ancient Ocean.

## EXPERIMENTAL SECTION

**Bulk crystallization and dissolution.** For the bulk growth experiments, the supersaturated solution contained 10.0 mM CaCl<sub>2</sub> and 10.0 mM NaH<sub>2</sub>PO<sub>4</sub> (Sigma-Aldrich, USA). 20.0 mM D- or L-Asp (Sigma-Aldrich, USA) was additionally added into the solution to examine their roles in brushite growth. The ionic strength was adjusted to 0.15 M using sodium chloride salts (Sigma-Aldrich, USA). The initial solution pH was adjusted to 5.60 using 1.0 M NaOH (Sigma-Aldrich, USA). 1.0 mg brushite crystallites (Acros, USA) were added into 250 ml solutions to initiate the seeded crystal growth. The crystal incubation period was 6 days without stirring. The grown crystals were observed directly under an optical microscope (Nikon, Japan).

For the brushite dissolution experiments, the large brushite crystals with the size of 100 μm were used, which were obtained from the above-mentioned bulk growth experiments in the absence of the amino acid. The undersaturated solution contained 4.00 mM CaCl<sub>2</sub> and 4.00 mM NaH<sub>2</sub>PO<sub>4</sub>. 20.0 mM D- or L-Asp was additionally added to examine the different roles of the enantiomers. The initial solution pH was adjusted to 5.60. The dissolution was initiated by adding the collected grown crystals (150 mg) into 250 ml undersaturated solutions. There was no stirring during the reaction, and the experimental period was 6 days.

To prevent bacterial contamination, each 250 ml reaction solution was treated with 0.25 g NaN<sub>3</sub> (Sigma-Aldrich, USA) prior to use. At the end of the experiments, the crystals were collected for examination by filtration using a 0.22 μm Millipore membrane.

**Chiral Adsorption.** Solutions with different super- or under-saturation, and containing 2.0 mM racemic amino acid (15 ml), were passed through 22 g of a brushite crystallite column (diameter of about 1 cm) at an average flow rate of 1 ml/h. The amount of brushite grown/dissolved during the column solution run was negligible. The original racemic solution, and the solution passed over the column, were examined by using reverse-phase high-performance liquid chromatography (RP-

HPLC). Standard curves of amino acid concentration vs. RP-HPLC peak areas are provided in Figures S1 and S2. Each adsorption experiment was repeated five times, in independent experiments. In order to examine the influence of solution condition on the chiral separation, solutions with different calcium and phosphate concentrations were used, and their compositions are listed in Table S1. For the supersaturation condition using equation 1, the values adopted for the dissociation constants of phosphoric acid were  $K_1 = 7.25 \times 10^{-3}$  M,  $K_2 = 6.31 \times 10^{-8}$  M and  $K_3 = 3.98 \times 10^{-13}$  M. The formation constants for the ion pairs CaH<sub>2</sub>PO<sub>4</sub><sup>+</sup>, CaHPO<sub>4</sub><sup>0</sup>, CaPO<sub>4</sub><sup>-</sup>, and CaOH<sup>+</sup> were taken as 28.1, 589,  $1.40 \times 10^6$  and 25.0 M<sup>-1</sup>, respectively.

To ensure that the observed chiral selection of Asp was controlled by the non-equilibrium states of brushite crystals in solution rather than by other factors including the existence of microbes within the experimental environment, variations in brushite crystallites and the enantiomeric ratio of Asp, great care was taken in each experiment to control these variables. For example, solutions were routinely treated by NaN<sub>3</sub> addition, heating, or UV irradiation prior to the synthesis and the adsorption experiments to exclude the influence of microbes. Additional experiments were repeated using brushite and Asp obtained from different sources (Table S2). In all cases, we found that the observations of chiral selectivity of brushite over Asp were independent of these variable treatments.

**RP-HPLC.** Solution samples were analyzed using a 1100 Series LC System (Agilent, USA) and a chiral column [Daicel Crownpak CR(+), Japan] with 195-205 nm UV detection at 0-25°C. The mobile phase was acidic water adjusted with HClO<sub>4</sub> to pH 1.00-2.00 for the chiral column. In order to examine the influence of solution conditions on the chiral separation, solutions with different calcium and phosphate concentrations were used; their compositions are listed in Table S1.

**Atomic force microscopy (AFM).** In situ AFM images were collected at room temperature (25°C) by using a multimode AFM (Veeco Nanoscope IVa, USA) on the {010} faces of both large brushite crystals with about 100 micrometers grown from original brushite crystallites and lab-synthetic brushite crystals with similar size in high supersaturated solution as described in reference 23, which were anchored inside a fluid cell. The solution conditions used during imaging were identical to the adsorption experiments. All images were acquired in contact mode. To reduce imaging artifacts, the tip force exerted on the surface was optimized.

**Computer simulations.** The structure parameters of brushite were adopted from the X-ray structure data at 300 K reported by Schofield,<sup>24</sup> with the unit cell parameters of  $a = 5.8105 \text{ \AA}$ ,  $b = 15.1758 \text{ \AA}$ ,  $c = 6.2337 \text{ \AA}$ , and  $\beta = 116.405^\circ$ . Widely

used OPLS-AA,<sup>25</sup> TIP-3P,<sup>26</sup> and A specially designed brushite force field were applied, which reproduced interfacial structure and hydration free energies well within that of experimental results. Molecular dynamics (MD) simulations were performed using the Gromacs 4.6.5 package.<sup>27</sup> The initial configurations of adsorbed Asp on steps were produced by the solute-parallel tempering simulation method.<sup>28</sup> The free energies profiles of the adsorption of D- and L-Asp molecules on the brushite [101] steps (step-A and step-B) were obtained by umbrella sampling with the weighted histogram analysis method (WHAM).<sup>29</sup> The adsorption free energy was obtained by the difference of the free energy at bulk solution and at the adsorbed state in the free energy minimum. For details, please see the Supporting Information(SI).

## RESULTS AND DISCUSSION

**Asymmetric effects of Asp on growing and dissolving brushite.** Bulk crystallization experiments show that brushite crystals in non-equilibrium states (growing or dissolving) have a distinct effect on the chiral recognition of Asp-enantiomers (Figure 1). In pure supersaturated solution, growing brushite crystals exhibited a trapezoidal habit with large {010} faces (Figure 1a). When D-Asp (20.0 mM) was added to the growth solution, the crystals became rectangular-shaped with much smaller diameter compared to triangular brushite crystals formed in the pure solution (Figure 1b). However, when L-Asp (20.0 mM) was added to the solution, the crystal morphology did not change significantly (Figure 1c); the crystal dimensions just became smaller. In undersaturated solutions, the morphology of dissolving brushite was also modified by the addition of Asp enantiomers (Figure 1e, g). However, the observed effect was reversed: that is, L-Asp played the dominated role in alternating morphology and the size of brushite crystals dramatically decreased, while the D-Asp had much less effect. In the presence of racemic Asp (20.0 mM), the growth morphology of brushite (Figure 1d) resembled that seen in the presence of D-Asp, and the dissolution morphology (Figure 1h) was analogous to that observed in the presence of L-Asp,

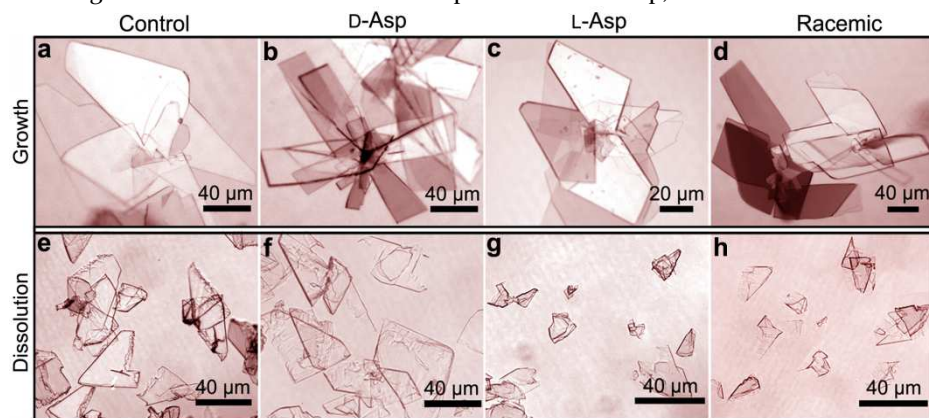


**Figure 1.** Optical images showing brushite morphology in supersaturated growth solution of (a) pure (no additives) and in the presence of 20.0 mM (b) D-Asp or (c) L-Asp or (d) racemic Asp, or in undersaturated dissolution solution of (e) pure (no additives) and in the presence of 20.0 mM (f) D-Asp, (g) L-Asp and (h) racemic Asp.

confirming that D- and L-enantiomers play the dominant role in brushite modification during growth and dissolution, respectively.

**Chiral separations of Asp on brushite in non-equilibrium states.** The above results indicate either that chiral Asp can selectively affect the growth and dissolution of brushite, or conversely, that the growing and dissolving brushite can recognize chiral Asp enantiomer. To test this hypothesis, we quantitatively determined the amount of adsorbed Asp enantiomers on brushite during both growth and dissolution by using RP-HPLC with a chiral column to measure the concentration of L- and D-Asp remaining in solution (Figures S1-S3). It should be mentioned that the errors for HPLC measurements from the standard curves (Figures S1 and S2) shows that the accuracy is sufficient to detect the chiral separation in our study cases. During the experiments, the solution pH was 5.60 and the ionic strength was kept at 0.15 M and the solution relative supersaturation,  $\sigma$ , is defined by eq. (1),

$$\sigma = \sqrt{\frac{\alpha_{Ca^{2+}} \alpha_{HPO_4^{2-}}}{K_{sp}}} - 1 \quad (1)$$

where,  $\alpha$  is the active concentration of the corresponding ions and  $K_{sp}$ , the solubility product of brushite,<sup>30</sup>  $2.57 \times 10^{-7} \text{ M}^2$ . The states of  $\sigma > 0$ ,  $\sigma = 0$  and  $\sigma < 0$  represent the solution conditions of supersaturation, saturation and undersaturation, respectively. At equilibrium condition ( $\sigma = 0$ ), we found the percent adsorbed on the solid phase for both enantiomers was the same at  $9.1 \pm 0.8\%$ . However, in supersaturated conditions ( $\sigma = 0.84$ ) (Figure 2a, and Figure S3), we found  $14.2 \pm 1.0\%$  of D-Asp and  $12.1 \pm 0.9\%$  of the L-Asp from the initial racemic solutions was present on the solid phase, giving an enantiomeric excess (*ee*) of about 8.0%. The balance of enantiomers was thus broken both on the crystal and in the solution. In undersaturated conditions ( $\sigma = -0.84$ ), the reduction in the

concentration of the D-enantiomer in solution was less than that for the L-enantiomer. The percentages of adsorbed D- and L-Asp on the solids were  $15.5 \pm 1.1\%$  and  $19.4 \pm 1.0\%$ , respectively (Figure 2a), and the *ee* value was about 11.2%. Thus more D-Asp adsorbed during growth, whereas more L-Asp bound during dissolution. The statistical analysis (using R Software, <https://www.r-project.org/>) showed that the *p*-value (one-tailed test) was less than 0.012 and the effect size was greater than 2.2, which supported the observation that the chiral selection was significant and

substantial. The magnitude of the chiral selectivity was strongly dependent on  $\sigma$  as demonstrated by the enantiomeric ratio ( $R$ ) of adsorbed L- to D-Asp (Figure 2b and Table S1), which shows that  $R$  decreased monotonically with increasing  $\sigma$ . This dependence shows that, by using the solution supersaturation as a control, the degree of chiral selection can be regulated and the resulting preference can be switched as a consequence of the dynamics of adsorption on the mineral rather than the structure of the mineral itself.

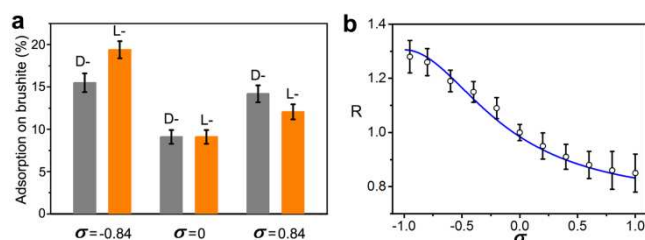


**Figure 2.**(a) Plot showing adsorption amounts of D- and L-Asp on the brushite surface in the supersaturated ( $\sigma=0.84$ ), saturated ( $\sigma=0$ ) and undersaturated ( $\sigma=-0.84$ ) solutions, respectively.(b) The ratio ( $R$ ) of L- to D-Asp adsorbed on brushite crystals at different supersaturation (open circle) and the model prediction (solid line).

**Chiral recognition between Asp enantiomer and brushite [101] steps on {010} facets.** The chiral enantiomer of amino acid selection observed in the bulk chemical and chromatographic analyses can be understood through microscopic *in situ* AFM examination of brushite growth and dissolution in the presence of the enantiomers.<sup>31-34</sup> The AFM images show that the brushite crystals grew and dissolved on complex screw dislocation hillocks and etch pits, respectively, on their large (0-10) facets. This clearly demonstrated the crystallization pathway of the classical crystal step movements. It is worthy to note that crystal growth via the non-classical cluster-attachment is usually characterized by its smaller step kinetic coefficient ( $\sim 10^{-5}$ - $10^{-4}$  cm/s), but the that of brushite is relatively high ( $\sim 10^{-1}$  cm/s, see details in SI).<sup>16,35-37</sup> Accordingly, the effect from smaller clusters in the chiral separation can be ignored in this system. The hillocks and pits both exhibited a triangular morphology, with steps propagating along the [101], [201] and [001] directions (Figure 3). Step edges along all directions were smooth when growing in pure solution (Figure 3a). While the addition of D-Asp altered all three step morphologies and lowered the step density. Among them, the [101] step was most strongly modified. It exhibited serrated and roughened edges, indicating a strong interaction between D-Asp with the step edge, thereby pinning the step, hindering step motion, and distorting the growth hillock (Figure 3b). However, the impacts of L-Asp on the growth steps were much less in comparison with those of D-Asp. Although there was a slight change in the terrace width

and step edges, the modifications to the step were isotropic with no pinning sites being apparent (Figure 3c). Under dissolution conditions, the dominant step modification was caused by L-Asp on the [101] step, which exhibited a loss of lateral stability (Figure 3f). The effect of D-Asp additives on the dissolution pits, however, was nearly negligible (Figure 3e). These observations suggest distinct enantiomer selection by the growing and dissolving [101] step in undersaturated and supersaturated conditions. In addition, it was found that the growth [101] step modulations were proportional to the D-Asp concentrations used, but they were not affected by L-Asp (Figure S4), thus demonstrating the specific recognition of D- rather than L-

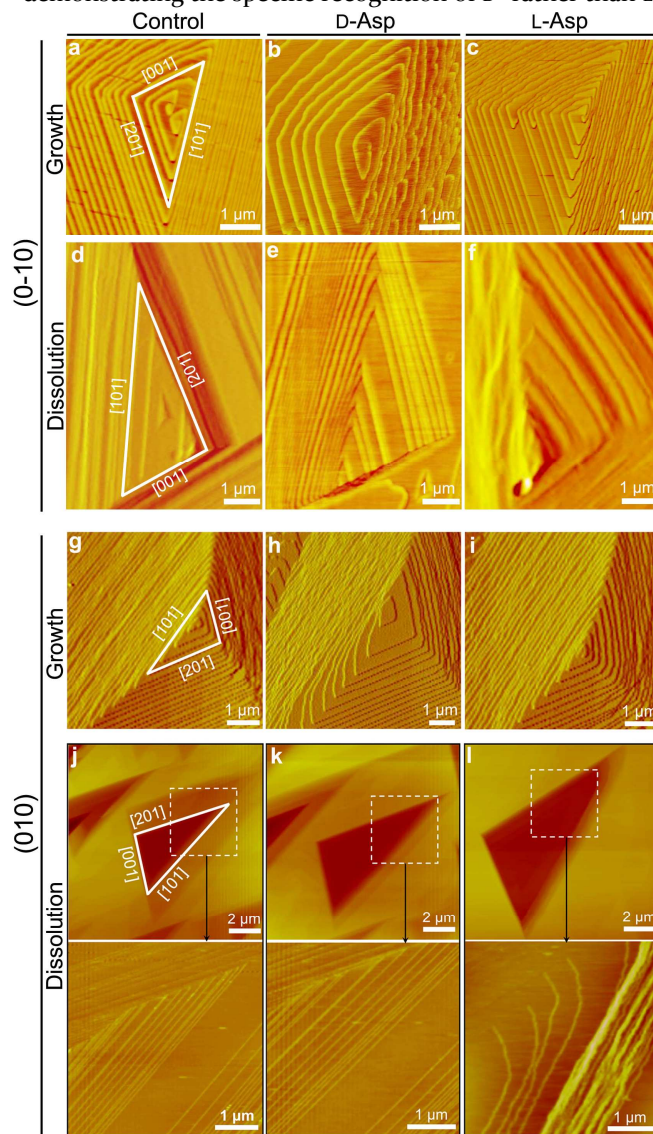


**Figure 3.** AFM images of active steps on the brushite (0-10, a-f) and (010, g-l) faces collected in supersaturated ( $\sigma=0.65$ , a-c, and g-i) and undersaturated solutions ( $\sigma=-0.69$ , d-f, and j-l). (a, d, g and j) In pure, non additive solution, (b, e, h and k) in the presence of 20.0 mM D-Asp, and (c, f, i and l) in the presence of 20.0 mM L-Asp.

1  
2 enantiomer. This result also confirmed that dynamic [101]  
3 steps did recognize Asp enantiomer in non-equilibrium  
4 state, and that chiral separation of Asp on brushite dy-  
5 namic surfaces is not caused by other factors such as con-  
6 tamination.

7  
8 Due to the mirror-symmetry found in crystals of brushite,  
9 if one face selects one enantiomer then theoretically, the  
10 selection should be reversed on the other face. However,  
11 our AFM examinations revealed that the chiral selection  
12 of Asp by [101] steps on (010) was identical to that on (0-10)  
13 faces (Figures 3). Using growth hillocks as an example, the  
14 [101] steps on both (010) and (0-10) faces were significantly  
15 modified by D-Asp, but their modification by L-Asp was  
16 insignificant (Figure 3a-c and Figure 3g-i). In the case of  
17 dissolution, it was L-Asp rather than D-Asp that became  
18 active in the [101] step modification on both (010) and (0-  
19 10) faces (Figure 3d-f, and Figure 3j-l). These facts imply  
20 that the dynamic [101] steps exhibited the same chiral  
21 characteristic on all {010} facets and the unexpected  
22 breaking of mirror-symmetry on the dynamic facets. Fur-  
23 thermore, if the mirror-symmetry remains during the  
24 brushite growth or dissolution in the presence of D- and L-  
25 Asp, the effect of D-Asp on (010) face should be the same  
26 as L-Asp on the (0-10) face. However, they were in fact  
27 different in the AFM observations (Figures 3, and Figure  
28 S5), further confirming the symmetry-breaking behavior.

29  
30 Previously, it has been noted that the mirror-symmetry of  
31 crystal facets is different from that of bulk symmetry of  
32 crystals in potassium bichromate ( $K_2Cr_2O_7$ ).<sup>38</sup> There are  
33 examples of systems where the macroscopic morphology  
34 of crystals shows a different symmetry than its space  
35 group, a feature known as "hypomorphism".<sup>39-41</sup> Although  
36 the exact reason for the facet symmetry-breaking is still  
37 unknown, one of the proposed possibilities relates to  
38 surface relaxation and reconstruction. Previously,  
39 brushite surface relaxation has been revealed and  
40 confirmed using surface X-ray diffraction,<sup>42</sup> which might  
41 lead to the symmetry-breaking of facets. Besides, the  
42 unequal average step densities of {010} faces of brushite  
43 and the reconstructed surface might also lead to the loss  
44 in mirror-symmetry of {010} faces. It should be  
45 emphasized that during dynamic crystal growth and  
46 dissolution, the surface of brushite crystal is under  
47 continuous surface relaxation and reconstruction, which  
48 may be attributed to the observed symmetry-breaking of  
49 the dynamic steps on {010} facets and exactly the same  
50 chiral selection behavior on both (010) and (0-10)  
51 dynamic faces. While the origin of mirror-symmetry  
52 breaking for crystal facets remains to be established,<sup>38-42</sup> it  
53 appears that investigation under dynamic brushite  
54 growth and dissolution conditions provides an excellent  
55 experimental case for further in-depth explorations and  
56 understandings.

**Configurations of dynamic brushite [101] steps in non-equilibrium states.** The different behaviors between D- and L-Asp on the growing and dissolving brushite crystals imply a new mechanism of chiral selection, which beyond our conventional understanding. Generally, such a chiral selection must be driven by a chiral crystal or its chiral faces. However, these chiral characteristics are previously concluded and understood by the crystals in their static states rather dynamic states.<sup>6-10</sup> In our case, although brushite crystals themselves do not display any chiral characteristic upon the current understanding, during the non-equilibrium growth and dissolution process the crystal steps are either under continuous construction or destruction, which are in a dynamic state rather than a static state. Given this, the previous understanding about chiral selection on static chiral crystals at the equilibrium state may in fact be invalid for the dynamic steps occurring at the transition states. Our following simulation study focuses on the dynamic steps in non-equilibrium states, and how they can lead to the chiral selection.

To engage in chiral selection, a broken symmetry in the structure of a step or face must exist.<sup>6,7</sup> Any brushite step including [101] on {010} facets consists of two calcium and phosphate ( $Ca-HPO_4$ ) layers (Figure 4a, and Figure S7). Unlike the [201] and the [001] steps, the calcium and phosphate ions in the [101] step form a zig-zag pattern (Figure S7). During crystal growth, the  $Ca-HPO_4$  unit will attach to the [101] step-edge on the second or the first layer, alternatively (Figure 4a), and thereby produce two different transient configurations. One is obtuse (step-A), and the other is acute (step-B) (Figure 4b). Before the ions can become incorporated, the desorption of water molecules from the surface, and the re-orientation and conformational adaptation of the  $Ca-HPO_4$  unit must occur, and therefore, there are incorporation barriers for the growth and dissolution of step-A and step-B (Figure 4c).

During both crystal growth and dissolution, the transitional step-A and step-B step must occur alternatively (Figure 4b). The overall transition rate from step-A to step-B, and vice versa, can be integrated for all the transition events ( $SI$ ). The length of step-A,  $L_{step-A}$ , is defined as the summation of all the [101] steps that are in state of step-A. When the overall transition rate from step-A to step-B equals that from step-B to step-A, the system reaches the steady state. Thus, the equilibrium ratio of the length of step-A and step-B can be determined from the difference in the transition barrier ( $\Delta\Delta G$ , see Figure 4c) and the chemical potential of the solution ( $\mu=kT\ln(1+\sigma)$ ) ( $SI$ ):

$$\frac{L_{step-A}}{L_{step-B}} = \frac{e^{\frac{2\mu + \Delta\Delta G}{kT}} + 1}{e^{\frac{2\mu}{kT}} + e^{\frac{\Delta\Delta G}{kT}}} \quad (2)$$

The ratio of  $L_{\text{step-A}}:L_{\text{step-B}}$  reflects the relative stability of step-A and step-B on the dynamic crystal surfaces. The change of the ratio with respect to supersaturation is provided in Figure 4d. In supersaturated solutions, the dominant (stable) configuration of the [101] step is step-A; in saturated solution, step-A and step-B are in equal probability, and in undersaturated solutions, the dominant (stable) configuration becomes step-B. The single crystal structure shows that the  $\text{HPO}_4^{2-}$  groups in the first and second surface layer orient differently, attributable to the twist of the  $-\text{OH}$  group connected to each phosphate group (see *SI* for details). Consequently, the different configurations of the steps in the two non-equilibrium states present different phosphate twists, thus creating the asymmetric structure needed for the chiral selection of amino acids. On [101] steps, these twisted  $-\text{OH}$  groups of phosphates are exposed to the solution and so are in-

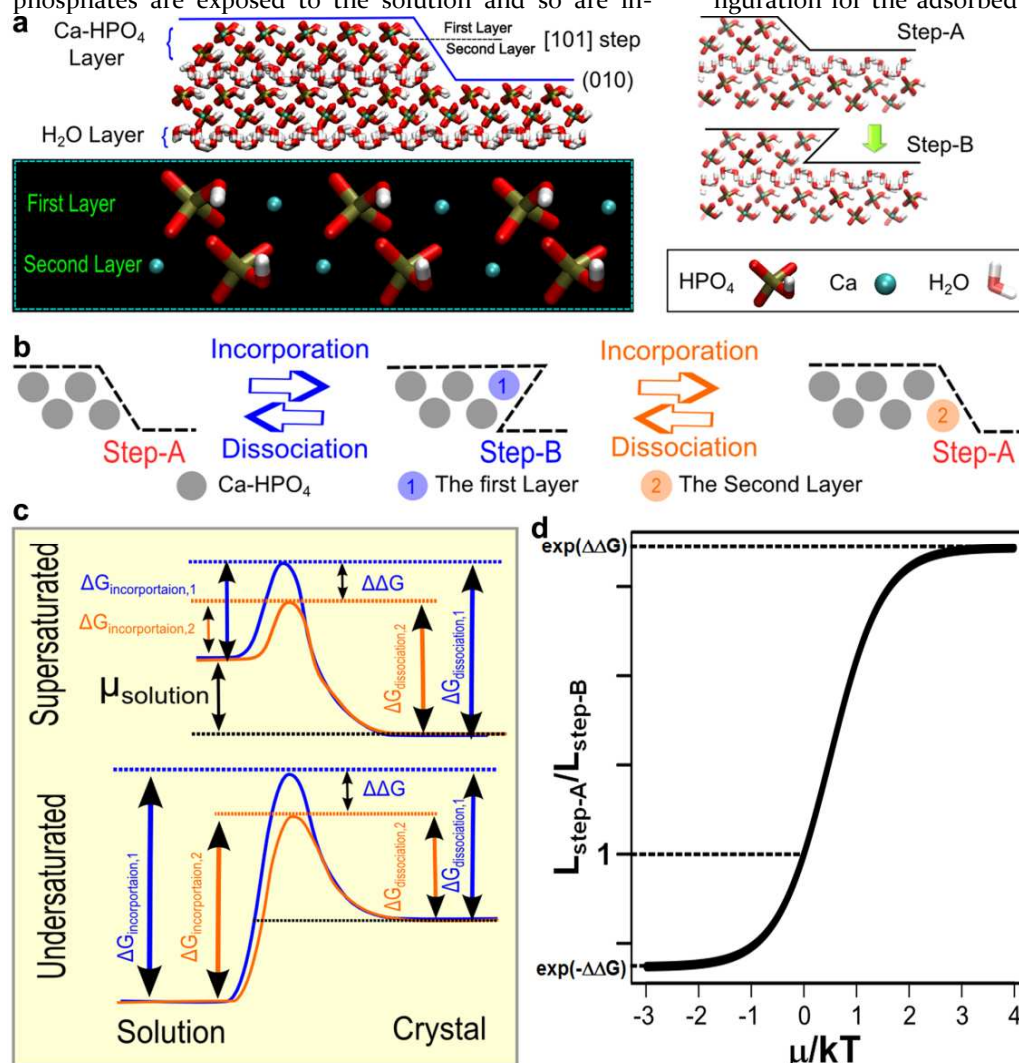


**Figure 4.** (a) Configurations of the brushite [101] step on {010} faces. (b) The transient configurations of the [101] step. (c) Barriers for the incorporation of the  $\text{Ca-HPO}_4$  unit to the [101] step edge on the first and the second layer. (d) Ratio of the length of step-A and step-B ( $L_{\text{step-A}}/L_{\text{step-B}}$ ) at different supersaturations ( $\mu = kT \ln(1 + \sigma)$ ).

involved in chiral recognition during the adsorption process. However, on the other two steps of the {010}, [201] and [001], the  $-\text{OH}$  groups of the phosphates are oriented inward towards the bulk crystal so they are not enrolled in the chiral adsorption process. This structural analysis corroborates the AFM observation that only the [101] steps exhibit chiral selection. Accordingly, it is reasonable to assume that the different transition states (step-A and step-B) of the [101] step is responsible for the enantiomer recognition of D- and L-Asp.

**Chiral selection of enantiomeric Asp by dynamic brushite [101] steps.** MD simulations were used to investigate the recognition of D- and L-Asp with the [101] steps with both the A and B configurations. The umbrella sampling with WHAM method was applied to calculate the adsorption free energy (see *SI* for details). The initial configuration for the adsorbed state was produced by parallel-

tempering MD simulation (to overcome the possible barriers among local free energy minimums). The free energy calculation (Figure 5a) indicates that on step-A, the adsorption free energy of D-Asp was  $-40.5 \pm 3.1$  kT, approximately 42% more than that of L-Asp ( $-28.5 \pm 2.3$  kT). In contrast, on step-B, the relationship between the binding energies was just opposite; L-Asp was preferred with an adsorption energy of  $-33.8 \pm 2.3$  kT as compared to  $-30.9 \pm 1.5$  kT for D-Asp. Hence, step-A prefers to adsorb D-Asp, and step-B prefers to adsorb L-Asp. As in the analysis above, the dominant configuration of the brushite [101] step for supersaturated solution is step-A, and for undersaturated solution is step-B (Figure 4d). Qualitatively, at high supersaturations, more D-Asp will be adsorbed, while at high undersaturations, more L-Asp will be adsorbed (Figure S9). This computer simulation result corroborates the experimental chromatograph analysis (Figure 2). Our calcula-

tions indicate that the dynamic switch of the [101] step configuration (from obtuse to acute) has a vital effect on the enantiomeric selection of Asp.

The analysis of the stable configuration of adsorbed Asp on steps indicates that the difference in binding free energy is attributable to stereochemical matching between the enantiomer and different configurations of the [101] step, especially the contribution of twisted phosphate on steps (Figure 5b). We found that D-Asp has three strong interaction points (either charge interaction or hydrogen bond interaction) with [101] step-A, while L-Asp has two interaction points (see snapshots in Figure 5b). Both D- and L-Asp have two interaction points on step-B, but the hydrogen bond distance of L-Asp with step-B is shorter than that of D-Asp (Figure S10). Clearly, subtle changes in step configuration have great impact on the interactions and the adsorption free energies of enantiomers with the step.

If a Langmuir adsorption model is applied, the fraction of step sites covered with D-Asp and L-Asp can be determined from their adsorption free energies (see SI for details), given the ratio of step-A to step-B which can be determined at any given supersaturation by Eq. 2. Of course, Asp can also adsorb on terraces on {010} faces and the other step edges ([001] and [201]) or other faces. As-

suming that the other faces and steps cannot separate L-Asp from D-Asp, we find that if assuming 15% of Asp is adsorbed on [101] step, the ratio of adsorbed L- to D-Asp on brushite predicted by this simple Langmuir model fit the experimental data well (Figure 2b).

**Possible roles of geological mineralization dynamics for achieving biochemical homochirality.** From synthetic organics, to biomedical pharmaceuticals, to the origin of life, the chiral selection of molecules presents both daunting challenges and significant opportunities in science and technology. Among the most promising avenues for chiral molecular discrimination is the adsorption of enantiomers onto chiral crystalline surfaces.<sup>6-10,43</sup> In this work, we found a different pathway, where solution environments can dynamically change the step configurations, and in the end, control the ability of mineral surfaces to effect chiral selection of amino acid enantiomers. This understanding should inform many technological applications where the establishment of a chiral switch-over, or chiral separation and purification, is critical.

Our study also points to a possible mechanism for generation of prebiotic biochemical homochirality. The mineral brushite is suggested to be one of the first precipitated rock-forming minerals in the acidic prebiotic ocean.<sup>18</sup> Before the appearance of life,

based on the models of early seawater,<sup>44-48</sup> the pH of ancient ocean increased from 5.8 in the Hadean ocean (4.3-Ga), which was stable for brushite, to 6.8 in the early Archean ocean (3.8-Ga), which would lead to the dissolution of brushite. Such a pH transition between the years 4.3-Ga and 3.8-Ga may lead to the alternation of the state of brushite from being in equilibrium to being in its dissolution state, which just happened to be the critical geological age for the appearances of biomolecules.<sup>49,50</sup>

Thus, L-amino acids in the prebiotic ocean could have been specifically enriched on these mineral surfaces. The preponderant existence of L-enantiomers likely provided more opportunities for asymmetric assembly and polymerization into L-peptides, and proteins. Generally, the conversion of amino acids into polypep-

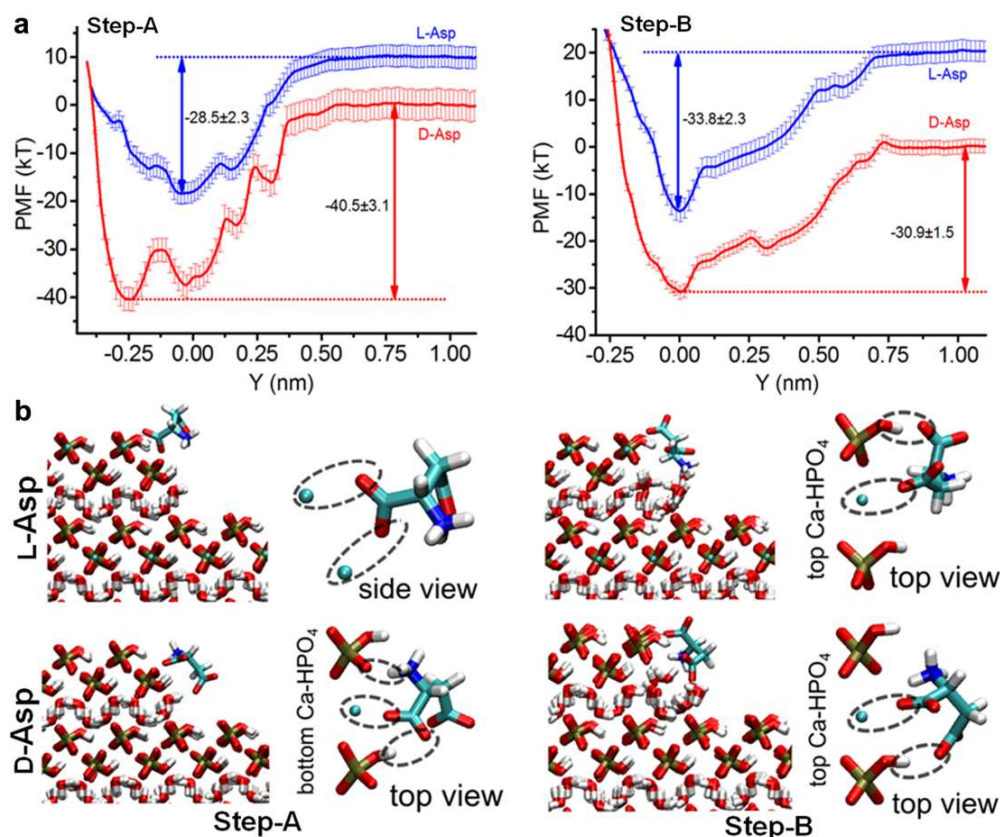


**Figure 5.** (a) Free energy profiles for the adsorption of D- and L-Asp on [101] step-A and step-B. (b) Snapshots of the stable configurations in the adsorbed state at free energy minimum.

tides on minerals is accepted as a possible chemical pathway in the formation of the precursors of life, which clearly would be a subsequent and significant milestone for the origin of life. More broadly, other minerals with similar switchable configurations of steps might also induce chiral selection via dynamic processes. Such an understanding fosters reconsideration of the roles of the earth's minerals in promoting prebiotic homochirality because of the natural dynamics of the prebiotic environment (e.g. mineralization and demineralization of rocks). Such notions must be taken into account when considering chiral enrichment from racemic solutions.

## CONCLUSION

In summary, we have demonstrated that the dynamic (rather than static) nature of materials can be a switch for chiral selection. A break of equilibrium at specific crystal-solution interfaces may lead to an asymmetric characteristic that provides an alternative strategy for chiral separation using step transition configuration, a feature that may have induced an evolution of organic chiral molecules. This molecular selection and evolution, based upon dynamic controls of substrate materials whose surface properties are regulated by pH, can provide an alternative strategy for chiral separation.

## ASSOCIATED CONTENT

Computer simulation methods, additional data, and supporting figures are included in Supporting Information. This material is available free of charge via the Internet at <http://pubs.acs.org>.

## AUTHOR INFORMATION

### Corresponding Author

\*rtang@zju.edu.cn

### Author Contributions

The manuscript was written through contributions by all authors. All authors have given approval to the final version of the manuscript. <sup>†</sup>W.J. and H.P. contributed equally to this work.

### Notes

The authors declare no competing financial interest.

## ACKNOWLEDGMENT

We thank Drs. J. J. De Yoreo and R. M. Hazen in particular for constructive discussions, and Drs. M. D. McKee, P. G. Falkowski and R. W. Friddle for their comments and suggestions. This work was funded by the National Natural Science Foundation of China (21625105 and 21571155) and the Fundamental Research Funds for the Central Universities of China (2012XZZX005). W.J. was supported by the Excellent Doctoral Student Supporting Program of Zhejiang University. S.R.Q.

acknowledges support under the auspices of the U.S. Department of Energy by Lawrence Livermore National Laboratory under Contract DE-AC52-07NA27344. R.T. was supported by the Talent Program of Zhejiang University.

## REFERENCES

- (1) Cronin, J. R.; Pizzarello, S. *Science* **1997**, *275*, 951–955.
- (2) Breslow, R.; Cheng, Z. L. *Proc. Natl. Acad. Sci. U.S.A.* **2009**, *106*, 9144–9146.
- (3) Cintas, P. *Angew. Chem., Int. Ed.* **2002**, *47*, 1139–1145.
- (4) Miller, S. L. *Science* **1953**, *117*, 528–529.
- (5) Zepik, H.; Shavit, E.; Tang, M.; Jensen, T. R.; Kjaer, K.; Bolbach, G.; Leiserowitz, L.; Weissbuch, I.; Lahav, M. *Science* **2002**, *295*, 1266–1269.
- (6) Hazen, R. M.; Sholl, D. S. *Nature Mater.* **2003**, *2*, 367–374.
- (7) Hazen, R. M. *Am. Mineral* **2006**, *91*, 1715–1729.
- (8) Lahav, N. *Biogenesis: Theories of Life's Origins*; Oxford Univ. Press: New York, 1999, pp 259.
- (9) Hazen, R. M. In *Progress in Biological Chirality*; Palyi, G.; Zucchi, C.; Caglioti L. Eds.; Oxford: Elsevier, 2004, pp 137–151.
- (10) Hazen, R. M.; Filly, T. R.; Goodfriend, G. A. *Proc. Natl. Acad. Sci. U.S.A.* **2001**, *98*, 5487–5490.
- (11) Fasel, R.; Parschau, M.; Ernst, K-H. *Nature* **2006**, *439*, 449–452.
- (12) Yun, Y.; Gellman, A. J. *Nature Chem.* **2015**, *7*, 520–525.
- (13) Bonner, W. A. *Origins Life Evol. Biosph.* **1995**, *25*, 175–190.
- (14) Frondel, C. *Am. Mineral* **1978**, *63*, 17–27.
- (15) Evgenii, K.; Wolfram, T. *Origins Life Evol. Biosph.* **2000**, *30*, 431–434.
- (16) Qiu, S. R.; Orme, C. A. *Chem. Rev.* **2008**, *108*, 4784–4822.
- (17) Kanzaki, N.; Onuma, K.; Treboux, G.; Ito, A. *J. Cryst. Growth.* **2002**, *235*, 465–470.
- (18) Gedulin, B.; Arrhenius, G. *Early life on earth*, Nobel Symposium 84 Bengtson, S. Eds.; Columbia Univ. Press: New York, 1994, pp 91–110.
- (19) William, J.; Hagan, J.; Amanda, P.; Steuerwald, A.; Hathaway, M. *Origins Life Evol. Biosph.* **2007**, *37*, 113–122.
- (20) Viedma, C. *Origins Life Evol. Biosph.* **2001**, *31*, 501–509.
- (21) Fox, S. W. *Science* **1960**, *132*, 200–208.
- (22) Addadi, L.; Weiner, S. *Proc. Natl Acad. Sci. U.S.A.* **1985**, *82*, 4110–4114.
- (23) Tang, R.; Darragh, M.; Orme, C. A.; Guan, X.; Hoyer, J. R.; Nancollas, G. H. *Angew. Chem., Int. Ed.* **2005**, *44*, 3698–3702.
- (24) Schofield, P. F.; Knight, K. S.; van der Houwen, J. A. M.; Valsami-Jones, E. *Phys.Chem. Miner.* **2004**, *31*, 606–624.
- (25) Jorgensen, W.L.; Maxwell, D.S.; Tirado-Rives, J. *J. Am. Chem. Soc.* **1996**, *118*, 11225–11236.
- (26) Jorgensen, W.L.; Chandrasekhar, J.; Madura, J. D.; Impey, R.W.; Klein, M. L. *J. Chem. Phys.* **1983**, *79*, 926–935.
- (27) Hess, B.; Kutzner, C.; van der Spoel, D.; Lindahl, E. *J. Chem. Theory Comput.* **2008**, *4*, 435–447.
- (28) Liu, P.; Kim, B.; Friesner, R. A.; Berne, B. J. *Proc. Natl. Acad. Sci. U.S.A.* **2005**, *102*, 13749–13754.
- (29) Kumar, S.; Rosenberg, J. M.; Bouzida, D.; Swendsen, R. H.; Kollman, P. A. *J. Comput. Chem.* **1992**, *13*, 1011–1021.
- (30) Dorozhkin, S. V.; Epple, M. *Angew. Chem., Int. Ed.* **2002**, *41*, 3130–3146.
- (31) Orme, C. A.; Noy, A.; Wierzbicki, A.; McBride, M. T.; Grantham, M.; Teng, H.H.; Dove, P. M.; DeYoreo, J. J. *Nature* **2001**, *411*, 775–779.

- 1  
2 (32) Cho, K. R.; Salter, E. A.; De Yoreo, J. J.; Wierzbicki, A.; El-  
3 hadj, S.; Huang, Yu.; Qiu, S. R. *Cryst. Growth Des.* **2012**, *12*,  
4 5939–5947.  
5 (33) Cho, K. R.; Salter, E. A.; De Yoreo, J. J.; Wierzbicki, A.; El-  
6 hadj, S.; Huang, Yu.; Qiu, S. R. *CrystEngComm*, **2013**, *15*, 54–64.  
7 (34) Scudiero, L.; Langford, S. C.; Dickinson, J. T. *Tribology*  
8 *Lett.* **1999**, *6*, 41–55.  
9 (35) Giocondi, J. L.; El-Dasher, B. S.; Nancollas, G. H.; Orme, C.  
10 A. *Phil. Trans. R. Soc. A.* **2010**, *368*, 1937–1961.  
11 (36) Onuma K.; Ito A.; Tateishi T. *J. Cryst. Growth.* **1996**, *1937*,  
12 773–776.  
13 (37) Onuma K.; Ito A. *Chem. Mater.* **1998**, *10*, 3346–3351.  
14 (38) Plomp, M.; van Enckevort, W. J. P.; Vlieg, E. *Phys. Rev.*  
15 *Lett.* **2001**, *86*, 5070–5072.  
16 (39) Shubnikov, A. Z. *Kristallogr.* **1911**, *50*, 19–23.  
17 (40) Reedijk, M. F.; Arsic, J.; Kaminski, D.; van Enckevort, W. J.  
18 P.; Vlieg, E. *Surf. Sci.* **2003**, *526*, 133–140.  
19 (41) Prywer, J. *CrystEngComm* **2009**, *11*, 196–202.  
20 (42) Arsic, J.; Kaminski, D.; Poodt, P.; Vlieg, E. *Phys. Rev. B*  
21 **2004**, *69*, 245406.  
22 (43) Bonner, W. A.; Kavasmaneck, P. R.; Martin, S. F.; Flores, J.  
23 *J. Science* **1974**, *186*, 143–144.  
24 (44) Caldeira, K.; Kasting, J. F. *Nature* **1992**, *360*, 721–723.  
25 (45) Kasting, J. F. & Ackerman, T. P. *Science* **1986**, *234*,  
26 1383–1385.  
27 (46) Walker, J. C. G. *Origins Life Evol. Biosph.* **1985**, *16*, 117–127.  
28 (47) Holland, H. D. *The Chemical Evolution of the Atmos-*  
29 *phere and Oceans*; Princeton: Princeton University Press, 1984.  
30 (48) Morse, J. W.; Mackenzie, F. T. *Aquat. Geochem.* **1998**, *4*,  
31 301–319.  
32 (49) Hagan, Jr, W. J.; Parker, A.; Steuerwald, A.; Hathaway, M.  
33 *Origins Life Evol. Biosph.* **2007**, *37*, 113–122.  
34 (50) Pasek, M. A. *Proc. Natl. Acad. Sci. U.S.A.* **2008**, *105*, 853–  
35 858.  
36  
37  
38  
39  
40  
41  
42  
43  
44  
45  
46  
47  
48  
49  
50  
51  
52  
53  
54  
55  
56  
57  
58  
59  
60

## TOC Graphic

